J Infrared Milli Terahz Waves (2013) 34:416–422
DOI 10.1007/s10762-013-9990-6

Measuring TE_1 mode Losses in Terahertz Parallel-Plate Waveguides

Marx Mbonye · Rajind Mendis · Daniel M. Mittleman

Received: 4 June 2013 / Accepted: 5 June 2013 /
Published online: 21 June 2013

1 Introduction

The parallel-plate waveguide (PPWG) has drawn considerable research interest [1–12], since it was first reported to support the undistorted propagation of broadband terahertz (THz) pulses. From that time, the transverse-electromagnetic (TEM) mode of the PPWG has been the popular choice for measurements due to its low loss, ease of quasi-optic coupling, and negligible dispersion as a result of the lack of a cutoff. Unlike the TEM mode, the lowest order transverse-electric (TE_1) mode has a cutoff frequency, and thus this mode was largely unexplored in the THz regime until recently [13, 14]. This recent work showed that the cutoff frequency could be moved to lower frequencies to reduce the dispersion by increasing the plate separation, while matching the input beam size to the plate separation to realize dominantly single-mode propagation. This same work predicted the possibility of realizing ultra-low ohmic losses in the dB/km range by again utilizing the TE_1 mode of this waveguide. These low ohmic losses could permit long-distance transport of THz radiation. However, with such long propagation distances a new concern arises: energy leakage out of the unconfined sides of the PPWG due to diffraction. In fact, this would be the dominant loss mechanism in the case under consideration, where the ohmic losses are virtually negligible.

We addressed this diffraction problem in a recent article [15], where we showed that it is possible to inhibit diffraction losses for the TE_1 mode by using a waveguide with slightly concave plates. Via a simple "bouncing plane wave" analysis, we demonstrated how to determine an ideal radius of curvature for the inner surfaces, for a waveguide operating at a given THz frequency. This is governed by a confocal condition, $R = {2b^2\nu}/{c}$, where R is the radius of curvature, b is the nominal plate separation, ν is the frequency, and c is the speed of light. We showed both experimentally and theoretically that for a waveguide with a plate separation of 1 cm, one could inhibit the diffraction at (and around) a frequency of 0.1 THz, when the inner surfaces of the PPWG have a radius of curvature of 6.7 cm. In this previous work, we used waveguides having a length of 25 cm, which is sufficient for

M. Mbonye · R. Mendis (✉) · D. M. Mittleman
Department of Electrical and Computer Engineering, Rice University, MS-378, Houston, TX, USA
e-mail: rajind@rice.edu

characterizing the propagating mode, but not long enough to determine the propagation loss. In this current work, we extend this idea to longer waveguides (as long as 167 cm). By employing a greater length, we attempt to measure the propagation losses; perhaps, at least determine an upper limit.

2 Experiment & Results

For the experiment, we fabricate two waveguides using polished aluminum plates. One of the waveguides has plates whose inner surfaces are curved along the transverse plane, with a radius of curvature of 6.7 cm, while the other waveguide has flat plates. Both waveguides are fabricated in segments, which can be assembled up to a maximum length of 167 cm. They have a transverse width (plate-width) of 3.8 cm, and are assembled with a constant center-to-center plate separation of 1 cm. Fig. 1(a) shows a schematic of the experimental setup. In the experiment, THz pulses are generated and detected using a conventional THz-time-domain-spectroscopy system based on fiber-coupled photoconductive antennas [16]. The THz receiver is shown scanning across the output face of the curved-surface waveguides. The input electric field is polarized parallel to the nominal plate surfaces to excite only TE modes. The input THz beam is centered on the front face in both the x and y directions and weakly focused to achieve a frequency-independent $1/e$ beam diameter of ~2 cm. This beam size was chosen to dominantly excite the TE_1 mode.

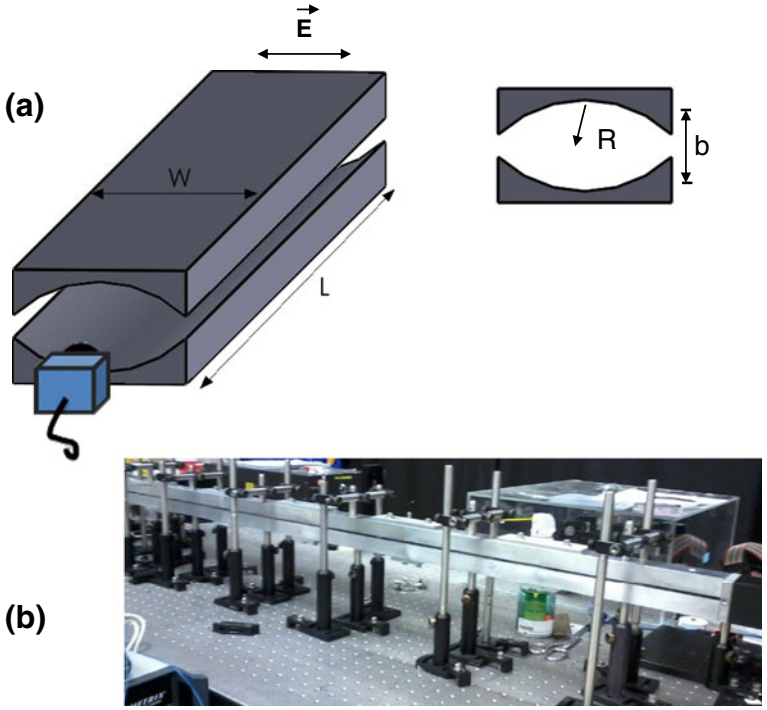

Fig. 1 (a) Schematic of the curved-surface waveguide where the input electric field is polarized parallel to the inner plate surfaces to excite the TE_1 mode. The THz receiver is shown scanning across the output facet. The inset shows the cross-sectional view of the waveguide. Note that the degree of curvature is exaggerated for clarity. (b) Photograph of the fully assembled curved-surface waveguide.

Fig. 1(b) shows a photo of the fully assembled curved-surface waveguide. A close look at the photo reveals the multiple sections of the waveguide, whose ends are carefully butt coupled using threaded stainless steel fasteners. This cascaded configuration allows us to reduce the length of the waveguide from 167 cm down to a length of 24 cm, in a piece-wise manner, for cut-back measurements [17].

Typical THz waveforms measured at the output of the 167 cm long flat-surface and curved-surface waveguides are shown in Fig. 2. For both measurements, the THz receiver is centered in both the x and y directions. The respective spectra (shown in the inset) indicate that there is significantly more signal content in the output corresponding to the curved-surface waveguide. This is consistent with an apparent reduction in the diffraction losses for the curved-surface waveguide, as predicted by the analytical and simulation results [15]. This plot also indicates that this curvature has the effect of confining a relatively broad range of frequencies, although the surface curvature was optimized for one particular frequency (0.1 THz). As in the previous case with the short length waveguides [15], a qualitative comparison of both output signals indicates that the residual group velocity dispersion introduced by the curved-surface waveguide is comparable to that introduced by the flat-surface PPWG.

We also image the electric field at the output facet of the waveguides in a plane perpendicular to the axis of propagation. The THz receiver is raster-scanned in a 20 × 60 mm^2 grid, in steps of 1 mm. The detected time-domain waveforms obtained from raster-scanning were Fourier transformed and their field amplitudes were used to plot two-dimensional (2D) color plots. Figs. 3(a) and (b) show 2D color plots at a frequency of 0.1 THz, all plotted on the same color scale. Fig. 3(a) illustrates the electric field distribution at the output facet of a 24 cm curved and flat-surface waveguide, while Fig. 3(b) shows the

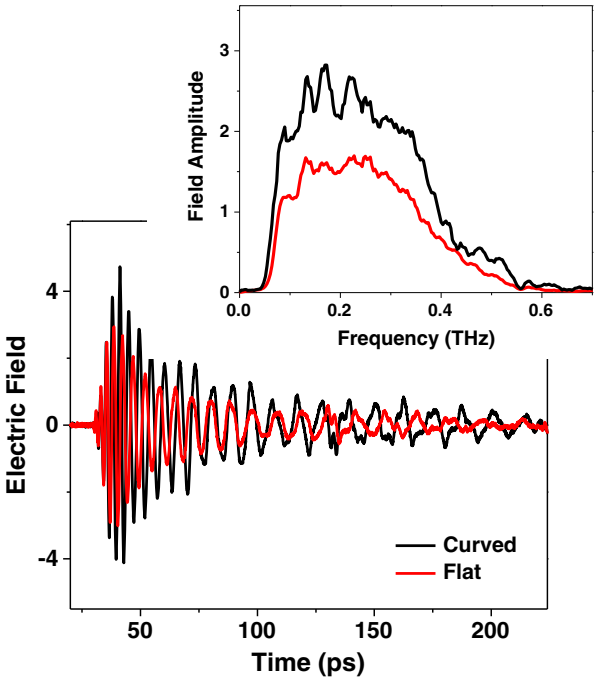

Fig. 2 Typical time-domain THz signals at the output of a flat-surface and curved-surface (R = 6.7 cm) waveguide measured on axis. The corresponding amplitude spectra are shown in the inset.

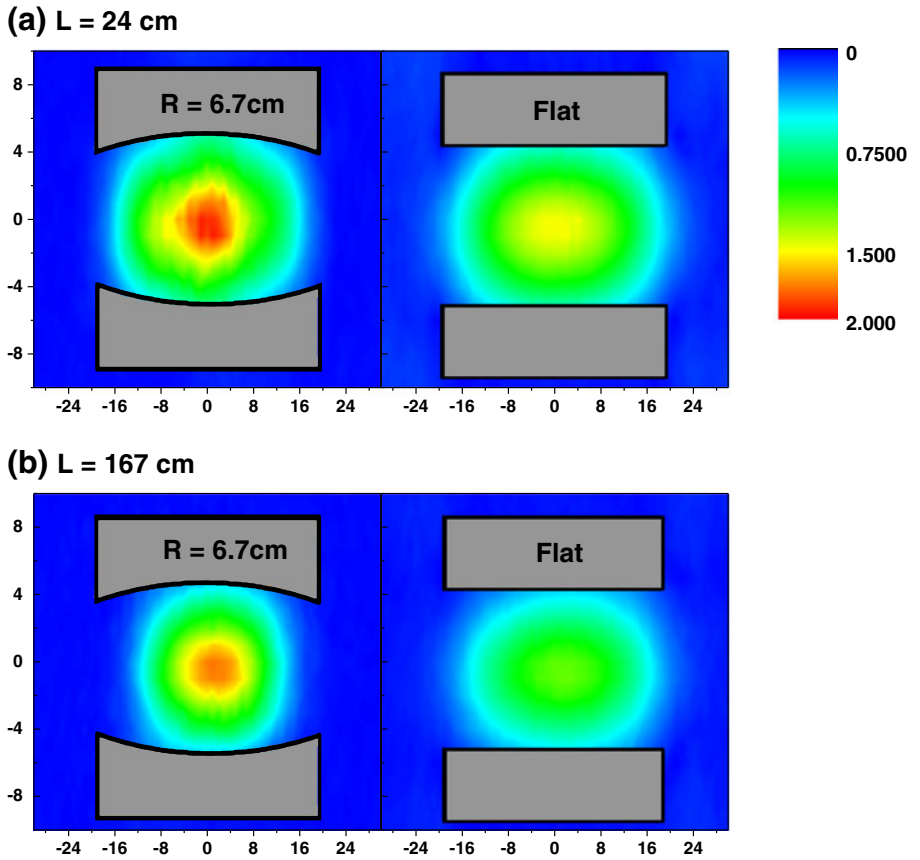

Fig. 3 Two dimensional color plots showing the electric field distribution at a frequency of 0.1 THz, measured across the output facet of (a) a 24 cm long curved-surface and flat-surface waveguide, and (b) a 167 cm long curved-surface and flat-surface waveguide. The grid dimensions are given in mm.

distribution at the output facets of 167 cm long waveguides. As with the previous case with the short-length waveguides [15], we observe a significant improvement in energy confinement in the curved-surface waveguide, whose curvature is optimized for a design frequency of 0.1 THz. It is interesting to note that the beam seems more confined at the end of the 167 cm long curved-surface waveguide, compared to the one at the end of the 24 cm long one. This is most likely due to the periodic nature of the variation of the beam size inside the waveguide (based on the bouncing plane wave argument), and not necessarily related directly to the longer propagation path length.

To quantify how much of the input power is dissipated by the time the THz signal arrives at the output end of the 167 cm long curved-surface PPWG, we perform Fourier transforms for the detected time-domain waveforms whose points are inside the 10×40 mm^2 grid shown in the inset in Fig. 4. We estimate the overall field intensity by summing the field intensity at each grid point. This is plotted in Fig. 4, as a function of frequency, along with that corresponding to the output of the 24 cm long one. Here, we observe a very clear reduction in the propagation loss in the vicinity of 0.1 THz (the design frequency) as expected, and a significant loss in power at higher frequencies.

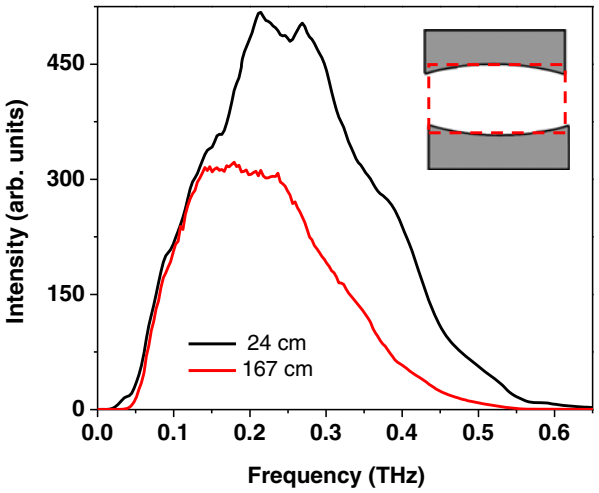

Fig. 4 Integrated intensity spectra of the measured waveforms at the output of the curved-surface waveguide, within a 10 × 40 mm grid as shown in the inset. The black and red curves correspond to a length of 24 cm and 167 cm, respectively.

Next, we quantify the power dissipated at various lengths along the waveguide for both the flat-surface and curved-surface waveguides. We select 6 lengths of interest: 167 cm, 143 cm, 95 cm, 71 cm, 47 cm, and 24 cm. Similar to the previous analysis, for each of these lengths, we perform Fourier transforms on the detected time-domain waveforms for the points inside a 10 × 40 mm^2 grid. As before, we estimate the overall intensity at each frequency by summing the intensities at each grid point. We perform several separate measurements and plot in Fig. 5 the mean of these measurements as symbolic points (normalized to the value at 24 cm). The error bars represent the standard deviation. The solid curves are exponential fits to the data points. For the curved-surface waveguide, we

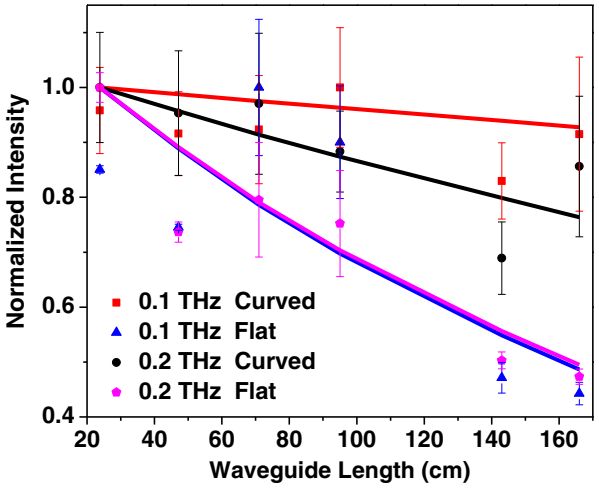

Fig. 5 Normalized integrated intensity at 0.1 THz and 0.2 THz, at specific points along the length of the flat-surface and curved-surface waveguides. The solid curves are exponential fits.

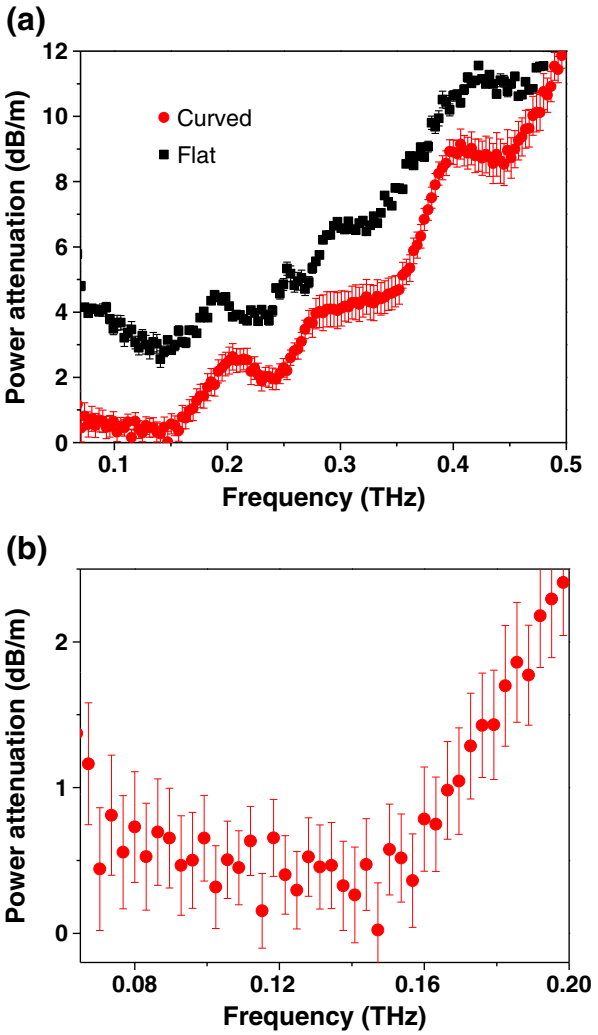

Fig. 6 (a) Estimated power attenuation for the curved-surface (red circles) and flat-surface (black squares) waveguides. (b) Zoomed in view of the range between 0.07 THz to 0.20 THz for the curved-surface waveguide.

observe a dramatic improvement in power conservation at the design frequency of 0.1 THz, and an appreciable amount of power conservation at a frequency of 0.2 THz. In contrast, close to 50% of the power is lost in the flat-surface waveguide at both 0.1 THz and 0.2 THz, by the time the propagating THz signal reaches the output of the 167 cm long waveguide.

Lastly, using the above intensity measurements corresponding to the various lengths, we derive the power attenuation in dB/m and plot this in Fig. 6(a), as a function of frequency. As expected, the loss for the curved-surface waveguide is lowest for frequencies in the vicinity of 0.1 THz. In order to better visualize the loss for the curved-surface waveguide near the design frequency, we zoom in the range between 0.07 THz to 0.20 THz and plot this in Fig. 6(b). This indicates that the power loss is about 0.5 ± 0.3 dB/m, in a spectral bandwidth of about 90 GHz around the design frequency. This value is somewhat smaller than the lowest loss measured (0.95 dB/m at 2.5 THz) for a THz waveguide in recent years [17],

although still much larger than the values obtained using an over-moded metallic circular waveguide at similar frequencies in the 1970s [18]. We note that previous theoretical results [13] have shown that this type of waveguide operating in the TE_1 mode can exhibit ultra-low ohmic losses, perhaps an order of magnitude lower than what is reported here (at this design frequency and plate separation). The measured higher loss could be attributed to experimental limitations, such as the discontinuities arising from the segmented waveguide geometry.

3 Conclusion

We have shown that it is possible to inhibit TE_1-mode diffraction losses in long PPWGs with slightly concave plates. We design a 167 cm long waveguide where the inner surfaces have a curvature of 6.7 cm, and demonstrate lateral energy confinement at (and around) a design frequency of 0.1 THz. Within experimental uncertainty, we estimate a power attenuation of about 0.5 dB/m in a spectral bandwidth of about 90 GHz around the design frequency.

Acknowledgments This work was supported in part by the National Science Foundation and by the Lockheed Martin Advanced Nanotechnology Center of Excellence at Rice University (LANCER).

References

1. R. Mendis and D. Grishkowsky, Opt. Lett. **26**, 846-848 (2001).
2. R. Mendis and D. Grischkowsky, IEEE Microw. Wireless Compon. Lett. **11**, 444-446 (2001).
3. H. Cao, R. A. Linke, and Ajay Nahata, Opt. Lett. **29**, 1751-1753 (2004).
4. S. Coleman and D. Grischkowsky, Appl. Phys. Lett. **84**, 654-656 (2004).
5. Z. Jian, J. Pearce, and D. M. Mittleman, Opt. Lett. **29**, 2067-2069 (2004).
6. J. Zhang and D. Grischkowsky, Opt. Lett. **29**, 1617-1619 (2004).
7. M. M. Awad and R. A. Cheville, Appl. Phys. Lett. **86**, 221107 (2005).
8. J. S. Melinger, N. Laman, S. S. Harsha, and D. Grischkowsky, Appl. Phys. Lett. **89**, 252220 (2006).
9. M. Nagel, M. Forst, and H. Kurz, J. Phys.: Condens. Matter. **18**, S601-S618 (2006).
10. Y. Zhao and D. Grischkowsky, IEEE Trans. Microw. Theory Tech. **55**, 656-663 (2007).
11. D. G. Cooke and P. U. Jepsen, Opt. Exp. **16**, 15123-15129 (2008).
12. N. Laman, S. S. Harsha, D. Grischkowsky, and J. S. Melinger, Biophys. J. **94**, 1010-1020 (2008).
13. R. Mendis and D. M. Mittleman, J. Opt. Soc. Am. B **26**, A6-A13 (2009).
14. R. Mendis and D. M. Mittleman, Opt. Exp. **17**, 14839-14850 (2009).
15. M. Mbonye, R. Mendis, and D.M. Mittleman, Opt. Exp. **20**, 27800-27809 (2012).
16. D. M. Mittleman, *Sensing with Terahertz Radiation* (Springer-Verlag, 2002).
17. B. Bowden, J. A. Harrington, and O. Mitrofanov, Opt. Lett. **32**, 2945-2947 (2007).
18. T. A. Abele, D. A. Alsberg, and P. T. Hutchison, IEEE Trans. Microw. Theory Tech. **23**, 326-333 (1975).